

G-Refine: A General Quality Refiner for Text-to-Image Generation

Chunyi Li¹, Haoning Wu², Hongkun Hao¹, Zicheng Zhang¹, Tengchaun Kou¹
 Chaofeng Chen², Lei Bai³, Xiaohong Liu^{1*}, Weisi Lin², Guangtao Zhai^{1*}
 Shanghai Jiao Tong University¹, Nanyang Technological University², Shanghai AI Lab³

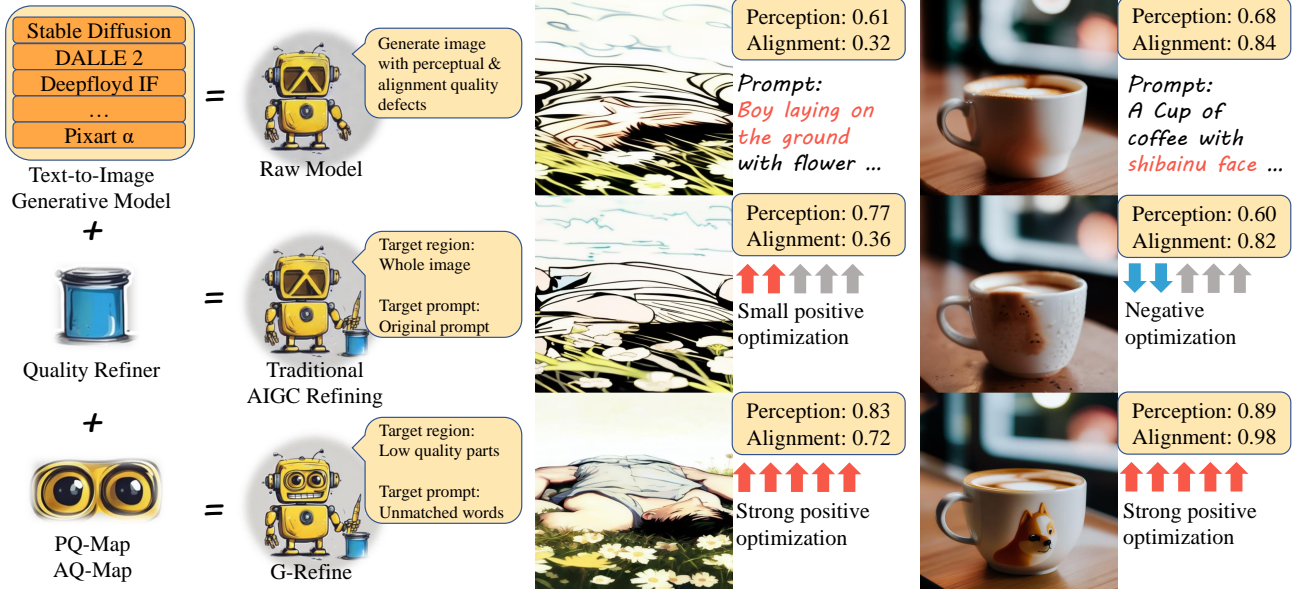


Figure 1: The original AIGIs from AIGIQA-20K, optimized by different refiners in terms of perceptual and alignment quality. Inspired by quality indicators, G-Refine better optimizes low-quality regions while avoiding affecting the high-quality regions.

ABSTRACT

With the evolution of Text-to-Image (T2I) models, the quality defects of AI-Generated Images (AIGIs) pose a significant barrier to their widespread adoption. In terms of both perception and alignment, existing models cannot always guarantee high-quality results. To mitigate this limitation, we introduce G-Refine, a general image quality refiner designed to enhance low-quality images without compromising the integrity of high-quality ones. The model is composed of three interconnected modules: a perception quality indicator, an alignment quality indicator, and a general quality enhancement module. Based on the mechanisms of the Human Visual System (HVS) and syntax trees, the first two indicators can respectively identify the perception and alignment deficiencies, and the last module can apply targeted quality enhancement accordingly. Extensive experimentation reveals that when compared to alternative optimization methods, AIGIs after G-Refine outperform in 10+ quality metrics across 4 databases. This improvement significantly contributes to the practical application of contemporary T2I models, paving the way for their broader adoption. The code will be released on <https://github.com/Q-Future/Q-Refine>.

CCS CONCEPTS

• Computing methodologies → Computer vision tasks.

*Corresponding Author


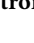

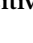
KEYWORDS














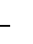






AI-Generated Content, Image Quality Assessment, Text-to-Image Alignment, Image Restoration, Syntactic Parsing

1 INTRODUCTION

Text-to-Image (T2I) generation models have revolutionized the production and consumption of visual content. These models, guided by free-form text prompts, aim to generate high perceptual quality images that closely match the text. Recent advancements in diffusion models have led to significant leaps in T2I capabilities, making AI-generated images (AIGIs) increasingly relevant for advertising, entertainment, and even scientific research. However, the quality of AIGIs varies significantly, hindering their widespread adoption in industrial production. According to Hugging Face, over 10,000 T2I models have been developed since 2024. While some advanced models can address the challenge of high-quality generation, their usage is much lower than that of mainstream models like Stable Diffusion (SD) 1.5. Older models deployed by users often yield subpar results due to their earlier development. Additionally, even the latest models like Playground v2.5 suffer from inconsistent generation performance, with both master-class artworks and Low-Quality (LQ) AIGIs coexisting.

To ensure high-quality T2I generation in the industry, several solutions are employed. The most common approach is multiple runs followed by manual selection, reporting only the best-quality AIGI.

Table 1: Using different optimizers for AI-Generated Images with low/high quality. [Keys:  strong positive,  positive,  zero,  negative optimization.]

Optimizer	Input	LQ optimization		HQ optimization	
		Percept	Align	Percept	Align
Restoration	Image				
Reconstruction	Image, text				
Refinement	Image, text	 	 		
Proposed	Image, text	 	 		

However, this method incurs significant computational waste and inevitable human labeling. More efficient methods include modifying T2I’s U-Net to improve the perceptual quality or adjusting the text encoder for better alignment, such as FreeU [36], TextCrafter [22], and DPT [30]. However, these methods require access to the original model’s parameters, making them only suitable for development rather than online consumption for the user end.

To overcome these challenges and facilitate the deployment of AIGI at the user end, a tailored optimization strategy is needed. This strategy should focus on generating images directly based on prompts, without relying on complex backend processes. However, there are three major obstacles: (i) Understanding the perception defects of AIGI. Unlike traditional Image Quality Assessment (IQA) [10, 17, 20, 56–59] methods that primarily address distortions such as blur and noise in Natural Sense Images (NSIs), AIGI’s defects stem from hardware limitations and technical limitations [18], like unnaturalness and artifacts. To accurately assess AIGI quality, a new approach is required to distinguish these unique types of artifacts. Moreover, beyond a single quality score, a pixel-level *perceptual quality map* is needed to locate spatial quality defects. Limited by spatial relationship knowledge, it’s difficult for existing IQA indicators to expand the overall score into a two-dimensional weight map. (ii) T2I alignment also requires similar maps instead of scores. The *alignment quality map* should indicate how well each part of the prompt corresponds to the generated image, and combine these insights into a comprehensive map. This task is more complex than simply assessing perceptual quality, as it involves understanding the semantic structure of the prompt. (iii) After identifying LQ regions, the challenge lies in optimizing them without compromising the quality of the rest of the image. *Optimization balancing* must be struck between applying just enough optimization to improve the image without introducing artifacts in High-Quality (HQ) regions. Thus, we propose G-Refine, a general quality optimizer as shown in Figure 1 with the following contributions:

PQ-Map: An accurate perceptual quality map indicator. It can accurately understand the connotation of the word “quality”, especially the quality defects of AIGIs. Considering the three quality-related factors (rationality, naturalness, and technical quality), it can accurately identify LQ regions for AIGIs. While outputting a 2D map, its performance can even ensemble single score models.

AQ-Map: An efficient alignment quality map indicator. By conducting syntactic parsing on a syntax tree, it can divide the prompt

into nodes representing different semantic information and analyze the relationship between the nodes. For nodes that do not align with the original AIGI, it uses the backtracking method to increase the weight of the ancestor node to give a complete alignment map.

Balanced-refiner: An optimization strategy for AIGI refiners. Inspired by PQ/AQ-Map, the refiner will **retain the HQ while improving LQ**. The model specifically consists of two stages. Stage 1 is similar to the traditional Refiner to fundamentally modify LQ; stage 2 refers to the restoration model by tuning LQ and HQ altogether. On 4 AIGI databases and 8 T2I generation models, compared to sota optimizers, G-Refiner has remarkable advantages in 9 perceptual quality and 4 alignment quality indicators.

2 RELATED WORKS

Without changing the internal generative model, to optimize AIGIs only through the prompt-image pairs, existing optimization strategies are mainly divided into the following categories as Table 1, which we summarize as three R’s.

Restoration: Treat AIGIs directly as NSIs by leveraging Super Resolution (SR) or Image Restoration (IR) algorithms through Convolutional Neural Networks (CNNs) based on prior knowledge. This method can improve the perceptual quality, but it does not support text modality as input. As the prompt cannot be used as a reference, the alignment quality is almost unchanged.

Reconstruction: A text-guided IR technique for AIGIs using the CLIP[31] model to encode prompts. This approach modifies low-level image features referring to the prompt, such as adjusting global brightness or altering the colors of an object, thereby enhancing alignment to a certain extent. However, its effectiveness is limited when dealing with LQ images, as it cannot significantly alter object structures. Similarly, when the alignment quality is poor, the model fails to generate non-existent objects from the prompt. Consequently, the overall optimization impact of this strategy is insufficient across both image quality dimensions.

Refinement: According to the prompt, AIGIs can be significantly modified at the semantic level. Among them, the conservative Refine strategy will denoise the image at a lower intensity. This cascade paradigm (generator + refiner) has been widely used in today’s T2I models, such as IF [7], SDXL [29], and SD Cascade [28]. A generator first provides a rough outline, then optimized through one or more refiners. A more radical strategy is to use the image directly as the starting point and perform the whole diffusion process. Compared with Reconstruction and Restoration, it can significantly optimize LQ regions. However, it usually contains certain AI artifacts, indicating an upper limit to its capabilities. While improving LQ, there will be negative optimization of HQ regions.

Therefore, distinguishing the LQ regions from the HQ is of great significance. However, though most of the existing IQA and T2I alignment indicators have excellent performance, their outputs are limited to a single score. Only Paq-2-Piq [51] supports the perceptual quality map and CLIP-Surgery [23] supports the alignment quality map. Unfortunately, the performance of these two methods is far inferior to the former, whose results are inconsistent with the subjective preference of the Human Visual System (HVS). Therefore, towards a targeted optimization of AIGIs, better quality map indicators are needed to inspire the refiner.

¹The perceptual and alignment quality is from Q-Align [45] and CLIPScore [31]. Normalized from 0 to 1.

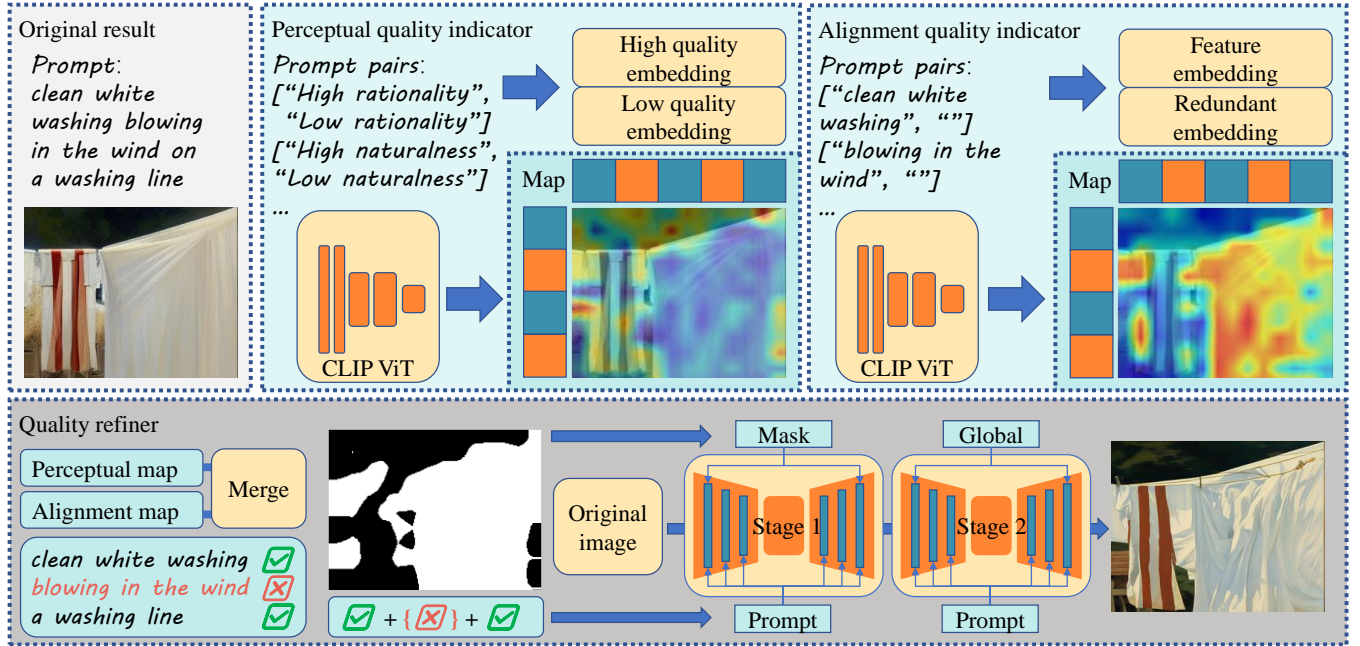


Figure 2: Framework of G-Refine, including a perceptual quality and an alignment quality indicator module. The refining process is targeted at optimizing unmatched prompts and both maps. The perceptual quality is optimized by introducing more texture while the alignment quality is improved by implementing “blowing in the wind” into the image.

3 PROPOSED METHOD

The framework of the proposed method is briefly illustrated in Figure 2, which includes a perceptual quality, an alignment quality indicator module for quality maps; and a quality refiner that merges quality maps spatially while emphasizing unmatched prompts semantically, towards a perceptual/alignment joint refinement.

3.1 Perceptual Quality Indicator

This PQ-Map module adjusts CLIP’s image and text encoders respectively, thereby obtaining the perceptual quality weight map of the image. Intuitively, using CLIP to find the region correlated with the word ‘high quality’ is the most direct method. However, existing research [33] reveals that CLIP tends to prioritize background over foreground, which contradicts the HVS mechanism. Therefore, referring to the solution of CLIP-Surgery [23], PQ-Map first changes CLIP’s original QKV self-attention into VVV:

$$C_I.QKV = \text{softmax}(V \cdot V^T \cdot \frac{1}{\|V\|_2}) \cdot V, \quad (1)$$

where V stands for value parameters for CLIP image encoder $C_I(\cdot)$ and I represents the original AIGI. Next, we also modify the text encoder. Existing Segmentation Model [13] can easily identify objects such as ‘cats’ and ‘dogs’. However, the ‘perceptual quality’ is different from the objective concept, which is a highly subjective concept that combines multiple factors. Therefore, the text encoder should not take “perceptual quality” directly, but decompose it into quality-related factors and encode them together. According to subjective analysis [4], AIGIs perceptual quality defects mainly include three categories: technical, rationality, and naturalness. On this

basis, a 4×2 token embedding with 512 length T_p is given:

$$T_p = C_T(t_0, t_1, t_2, t_3), \quad (2)$$

where the text encoder $C_T(\cdot)$ process the text pairs of CLIPQA [39] t_0 representing the overall perceptual quality, and text pairs t_{1-3} for three perceptual quality defects. Generally, the perceptual quality follows the cask effect. The excellence of a single factor cannot guarantee a score improvement, but its defects will inevitably lead to a decrease. Thus we express the perceptual quality map P and the score p as:

$$\begin{cases} L_{raw} = C_I \odot (T_p[:, 0] - T_p[:, 1]) \\ L_{per} = L_{raw}[0] \cdot \prod_{i=1}^3 \min(\frac{L_{raw}[i]}{\alpha[i]}, 1) \\ P = \text{BIC}(L_{per}), p = L_{per}[0], \end{cases} \quad (3)$$

where $L_{(raw, per)}$ stands for the raw logit embedding, and final perceptual quality embedding combined with four logits. $\text{BIC}(\cdot)$ rescales the logit into the size of I from bi-cubic interpolation. Logits below α will introduce a penalty to L_{per} . From the difference between p and subjective quality annotation, PQ-Map can update T_p to a better embedding, in order words, to fully interpret the complex connotation of the word ‘perceptual quality’, as shown in Figure 3.

In the subsequent quality map calculation, the token embedding layer can be disabled, without extracting any text features, but directly input the features T_p representing the perceptual quality into the text encoder. Figure 4 shows the map results using the original CLIP or the improved encoder. The map obtained from the original image encoder has almost no regularity and only shows high correlation at a few meaningless points; after improving the image

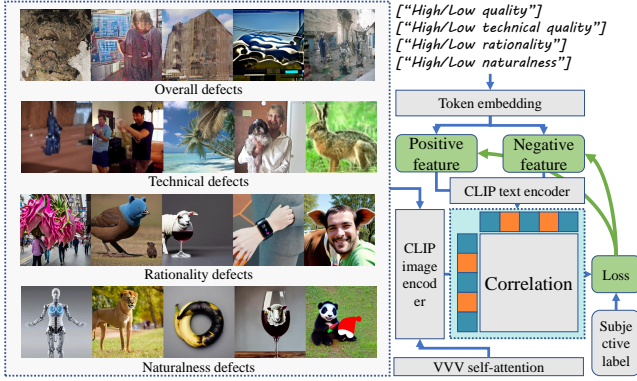


Figure 3: Using overall perceptual quality, and (technical, rational, natural) defected images to train the CLIP model. Both image and text encoder are modified in terms of self-attention and token embedding.

encoder, the original text encoder can perform certain semantic segmentation of the image, but due to the limited understanding of ‘perceptual quality’, it cannot mark all LQ regions and might even reverse LQ and HQ. An accurate perceptual quality map is available only by applying two improved encoders simultaneously. The results above prove the modifications of the two encoders bring significant positive effects jointly to the perceptual quality map.

3.2 Alignment Quality Indicator

This AQ-Map module first decomposes the prompt into phrases with different semantic meanings, analyzes the T2I alignment of each phrase, and finally merges them to obtain an alignment quality map for the whole prompt. Considering the length of prompts and complex subordination relationships between words, it is unrealistic to directly input prompts into C_T to calculate alignment. Therefore, we build a syntax tree $Tree$ from the NLTK(\cdot) package, using nouns pns as the clustering center, and assign each tree node to different phrases phs :

$$\begin{cases} Tree = \text{NLTK}(prompt) \\ phs = pns = Tree.Noun \\ phs[j].append(Tree[||pns[j], Tree||_{\min}]), \end{cases} \quad (4)$$

where $prompt$ is the original input prompt. The phs is initialized as noun nodes pns , while the remaining nodes will be associated with the closest pns to form several different phrases. The above method effectively segments prompts, at the cost of destroying the syntax tree. To solve this problem, according to the original dependency relationship of pns , AQ-Map allocates a new ancestor ans for each phs using the Algorithm 1. After segmentation, AQ-Map calculates the alignment quality map and score (A_{phs}, a_{phs}) for each phrase separately:

$$\begin{cases} A_{phs}[j, :] = \text{softmax}(C_I(I) \odot C_T(phs[j], "")) \\ a_{phs}[j] = A_{phs}[j, 0], \end{cases} \quad (5)$$

where index $j \in [0, \text{len}(phs) - 1]$. pns experience a similar computation with (A_{pns}, a_{pns}) . An empty string “” is encoded as redundant

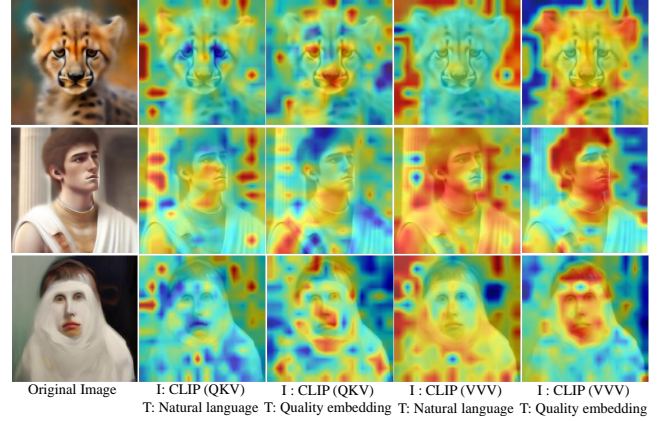


Figure 4: Visualization result of the perceptual quality map, using the original CLIP or improved image/text encoders. The original image encoder generates meaningless results while the original text encoder labels reversely. Reasonable results are available only when two encoders are modified.

feature and removed by $\text{softmax}(\cdot)$. Therefore, AQ-Map can summarize the alignment defect into the following two types, with typical examples shown in Figure 5:

- Noun unmatched: $a_{pns} < a_{bound}$ which indicates the noun doesn’t exist in the image. Here, the whole phrase should be drawn on the correlated region of its ancestor node.
- Adj. unmatched: $a_{phs} < a_{pns}$ which means the noun exists, but adjectives are not well-represented on it. In this case, the phrase should be drawn on the region itself.

Thus, initialize the overall alignment quality map $A = 1$, AQ-Map implement the weight of A_{pns} on A as:

$$A = \begin{cases} A \cdot A_{pns}[j] & a_{pns} < a_{bound} \\ A \cdot A_{pns}[phs[j].ancestor] & a_{phs} < a_{pns}. \end{cases} \quad (6)$$

For all index j with two alignment defects above, the phrases are also emphasized in the prompt for stronger refining strength:

$$prompt = prompt + 0.1phs[j]. \quad (7)$$

Then following the cask effect same as equation (3), the alignment quality score a will be:

$$a = C_I(I) \odot C_T(prompt) \prod_j \min(\frac{a_{phs}[j]}{\beta}, 1), \quad (8)$$

where for each phrase, alignment score below β will introduce penalty to a . From this, AQ-Map emphasized the phrases unaligned with the original image and mapped their corresponding regions that needed improvement based on the alignment defects.

3.3 Quality Refiner

The quality refiner is designed to optimize the image for both perceptual and alignment quality. This model is cascaded by a refinement and a restoration stages, the former conducts a strong denoising process according to the map and score given above, and the latter performs a mild denoising globally. Since the targeted

Algorithm 1 get_phrase_ancestor

```

1: function GET_PHRASE_ANCESTOR(pns, phs, Tree, obj)
2:   ans, stack  $\leftarrow$  {}, {}
3:   for pn in pns do
4:     ans[pn]  $\leftarrow$  pn
5:     for ph in phs do
6:       stack[ph]  $\leftarrow$  pn
7:   pq  $\leftarrow$  [Tree.root]
8:   while pq is not empty do
9:     obj  $\leftarrow$  pq.head
10:    for child in obj.children do
11:      pq.add(child)
12:      if stack[child.ancestor]  $\neq$  stack[child] then
13:        find the first ancestor with tag "NOUN"
14:        for ancestor in child.ancestor do
15:          if ancestor.pos == "NOUN" then
16:            ans[stack[child]]  $\leftarrow$  stack[ancestor]
17:            break
18:    pq.dequeue
19:  return ans

```

refining region has a relatively lower quality and more alignment defects, the probability densities for two stages are z_1/z_2 :

$$\begin{cases} z_1 = \frac{p+a}{2} \cdot \text{QKV}(\text{prompt}, \text{Bi}(1 - P + A)) \\ z_2 = \delta \cdot \text{QKV}(\text{prompt}, 1), \end{cases} \quad (9)$$

where the strength of z_1 depends on quality (p, a) while z_2 takes a extremely small strength δ . $\text{Bi}(\cdot)$ binarizes the map into a mask. After obtaining the probability densities, we can denoise the image with the refined result R :

$$R = \mathcal{D}_{n_2}^{z_2} \cdots \mathcal{D}_1^{z_2} (\mathcal{D}_{n_1}^{z_1} \cdots \mathcal{D}_1^{z_1} (I)), \quad (10)$$

where \mathcal{D}_n^z denotes the diffusion operation at the n -th iteration and (n_1, n_2) are the specific diffusion steps for each stage.

4 EXPERIMENT

4.1 Validation Databases

To assess the efficacy of the proposed G-Refine method across diverse generative models, we conducted performance evaluations on four commonly used AIGI databases: DiffusionDB [41], Gen-Image [60], AGIQA-1K [55], and AGIQA-3K [21]. Considering the huge scale of the first two, we randomly selected 3,000 images for refining, while using the complete set for the latter two. Since these AIGIs only come from traditional models like SD1.5, to verify our versatility for other generative models, we randomly generated 500 images each by 8 commonly-used models² for our G-Refine pipeline to optimize. Besides the whole G-Refine, we adopt the subjective scoring result from the two most popular AIGI quality databases, AIGIQA-20K [16] (testing set³) and AIGIQA-3K (full set) [21], to validate the effectiveness of PQ/AQ-Map quality indicators. These databases contain fine-grained Mean Opinion Score (MOS) as

²The 8 models are selected by the download times on huggingface. For some other advanced models with less popularity, the refining result is attached in the supplementary.

³Split as NITRE 2024 Challenge. [15, 26]

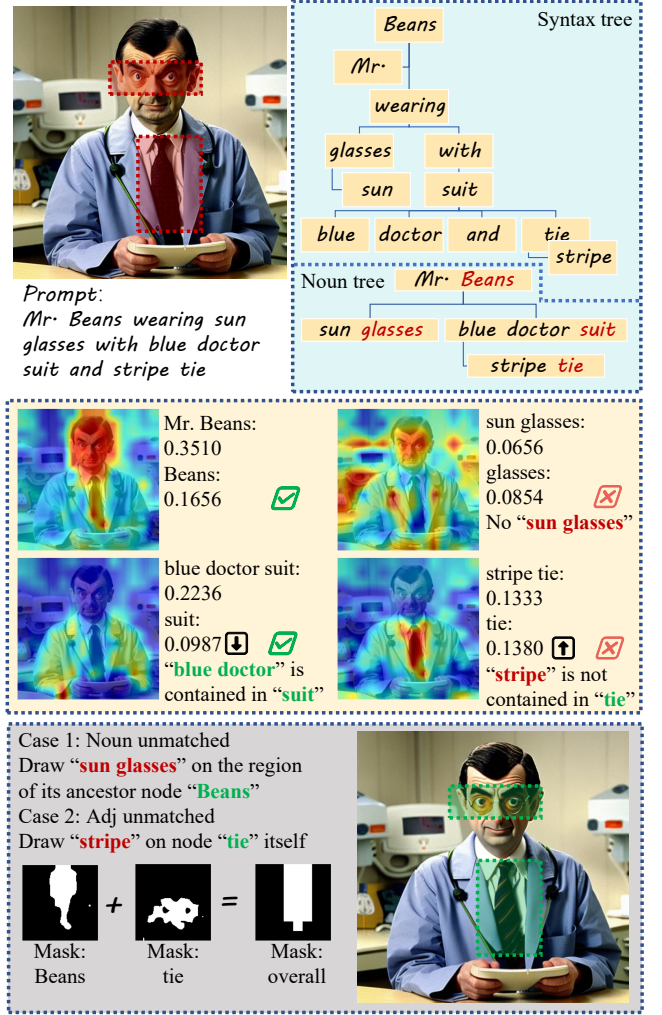


Figure 5: The mechanism of identifying alignment quality defects. Include syntax tree construction, quality defect identification, and mask processing. Both unmatched nouns and adjectives can be enhanced on their correlated region.

perceptual and alignment quality labels, to measure the correlation between them and objective evaluation results.

4.2 Experiment Settings

For quality optimization, we include 13 representative methods in different categories as baselines, including (**Restoration**): RFDN [25], Swin2SR [5], StableSR [40], and DASR [42]; (**Reconstruction**): SD-Upscale [34], Instructpix2pix [1], DiffBIR [24], PASD [50]; and (**Refinement**): SDXL-Refiner [29], SD (full-model) [34], SDXL (full-model) [35], InstructIR [6], and Q-refine [19]. All models are run by 20 iterations for a fair comparison. The optimization quality is comprehensively evaluated in 13 indicators, namely four (**Perceptual**)⁴: CLIPQA [39], UNIQUE [53], LIQE [54], DBCNN [52], TOPIQ [2], CNNIQA [11], MUSIQ [12], BRISQUE [27], Q-Align [45]; and nine

⁴FID is not considered as it shows less correspondence with human preference.

Table 2: Using different quality optimizers on GenImage database. Abbreviations: BRISQ: BRISQUE; CLIPS: CLIPScore; ImgRw: ImageReward; PicS: PicScore. Left/right for perceptual/alignment quality. [Key: **Best; **Second Best**; **Negative optimization**].**

Optimizer	Method / Indicator	CLIPQA↑	UNIQUE↑	LIQE↑	DBCNN↑	TOPIQ↑	CNNIQA↑	MUSIQ↑	BRISQ↓	Q-Align↑	CLIPS↑	ImgRw↑	PicS↑	HPSv2↑
N/A	<i>Original Images</i>	0.6911	1.1634	3.6417	0.6004	0.5605	0.6347	66.337	17.344	3.9609	0.9809	0.0724	0.7117	0.2563
Restoration	RFDN (ECCV2020)	0.6558	1.1119	3.5193	0.5579	0.5176	0.6225	65.416	22.748	3.8633	0.9830	0.0479	0.7027	0.2556
	Swin2SR (ECCV2022)	0.6982	1.1651	3.6435	0.6021	0.5617	0.6346	66.378	17.379	3.9609	0.9807	0.0721	0.7124	0.2563
	StableSR (Arxiv2023)	0.7306	1.3611	3.9148	0.6639	0.6441	0.6497	71.360	14.595	3.9883	0.9807	-0.0577	0.6858	0.2574
	DASR (CVPR2021)	0.6345	0.8340	2.8897	0.6309	0.5205	0.6921	61.111	53.082	3.4648	0.9784	-0.0349	0.6498	0.2533
Reconstruct-ion	SD-Upscale (CVPR2022)	0.6655	1.1363	3.5722	0.5335	0.5178	0.5998	66.119	24.979	3.8574	0.9835	0.0373	0.6993	0.2558
	Instructpix (CVPR2023)	0.6204	0.8441	3.0683	0.5098	0.4791	0.5588	61.714	26.031	3.7422	0.9814	0.0255	0.6701	0.2562
	DiffBIR (Arxiv2024)	0.7313	1.1327	3.6557	0.6113	0.5853	0.6436	65.987	11.505	3.9297	0.9843	-0.1569	0.6769	0.2542
	PASD (Arxiv2024)	0.7214	1.3444	4.0707	0.6534	0.6501	0.6280	69.691	13.852	4.0156	0.9845	0.0038	0.7358	0.2565
Refinement	SDXL-Refiner (ICLR2023)	0.6068	0.9338	3.2709	0.4932	0.4723	0.5062	62.343	30.049	3.8672	0.9841	0.2027	0.7153	0.2571
	SD (CVPR2022)	0.6110	0.8163	2.9576	0.4903	0.4636	0.4212	60.341	24.632	3.6191	0.9335	0.0013	0.6591	0.2545
	SDXL (ICLR2024)	0.6390	0.9696	3.3239	0.5074	0.4968	0.5846	63.598	28.300	3.9355	0.9918	0.2683	0.7652	0.2578
	InstructIR (Arxiv2024)	0.6866	1.0776	3.5751	0.5819	0.5566	0.6371	64.668	28.945	3.8867	0.9871	-0.0395	0.6680	0.2542
	Q-Refine (ICME2024)	0.7358	1.1833	3.7128	0.6122	0.5877	0.6491	66.943	11.630	3.9668	0.9889	-0.1109	0.6818	0.2548
G-Refine (Ours)		0.7444	1.5139	4.1280	0.6817	0.6679	0.6603	73.004	11.225	4.3366	0.9906	0.2290	0.7656	0.2604

Table 3: Using different quality optimizers on DiffusionDB database. Abbreviation and keys follow Table 2.

Optimizer	Method / Indicator	CLIPQA↑	UNIQUE↑	LIQE↑	DBCNN↑	TOPIQ↑	CNNIQA↑	MUSIQ↑	BRISQ↓	Q-Align↑	CLIPS↑	ImgRw↑	PicS↑	HPSv2↑
N/A	<i>Original Images</i>	0.7147	0.9106	3.5127	0.6094	0.5714	0.6263	65.003	15.093	3.8672	0.9822	-0.1085	0.7372	0.2550
Restoration	RFDN (ECCV2020)	0.7147	0.9117	3.5127	0.6093	0.5714	0.6256	65.004	15.076	3.8672	0.9822	-0.1089	0.7372	0.2550
	Swin2SR (ECCV2022)	0.7125	0.9122	3.5156	0.6103	0.5725	0.6265	65.004	15.093	3.8711	0.9824	-0.1089	0.7371	0.2550
	StableSR (Arxiv2023)	0.6920	1.1946	3.5930	0.6458	0.6045	0.6301	69.200	16.035	3.8789	0.9637	-0.2011	0.6592	0.2551
	DASR (CVPR2021)	0.6411	0.4695	2.8614	0.6526	0.5802	0.6811	61.413	15.539	3.4785	0.9781	-0.1997	0.7016	0.2552
Reconstruct-ion	SD-Upscale (CVPR2022)	0.6576	0.9454	3.4477	0.5756	0.5459	0.5837	65.256	14.392	3.8340	0.9724	-0.1393	0.7302	0.2545
	Instructpix (CVPR2023)	0.6325	0.6157	3.2975	0.5007	0.4739	0.5056	59.299	16.236	3.6270	0.9690	-0.1068	0.7001	0.2542
	DiffBIR (Arxiv2024)	0.7111	0.9046	3.2790	0.5691	0.5238	0.6265	67.302	11.438	3.8152	0.9784	-0.1835	0.7057	0.2547
	PASD (Arxiv2024)	0.7047	1.3098	3.7973	0.6393	0.6568	0.6436	67.146	16.468	3.8215	0.9819	-0.1836	0.6721	0.2517
Refinement	SDXL-Refiner (ICLR2023)	0.5602	0.4098	2.8306	0.4973	0.4426	0.4613	61.377	14.429	3.5816	0.9686	0.0380	0.6948	0.2517
	SD (CVPR2022)	0.6553	0.6896	2.7884	0.4896	0.4611	0.4816	59.392	21.925	3.5996	0.9438	-0.0269	0.6961	0.2549
	SDXL (ICLR2024)	0.6203	0.7874	3.7208	0.5772	0.5501	0.5899	63.440	15.161	3.9785	0.9895	0.1402	0.7861	0.2575
	InstructIR (Arxiv2024)	0.7370	0.9459	3.6083	0.6402	0.6181	0.6410	63.179	15.192	3.9414	0.9863	-0.1738	0.7111	0.2529
	Q-Refine (ICME2024)	0.7194	1.0040	3.4199	0.5981	0.5593	0.6431	66.085	12.018	3.9336	0.9915	-0.1834	0.6728	0.2533
G-Refine (Ours)		0.7153	1.4706	3.8922	0.6762	0.6471	0.6569	72.193	13.934	4.2034	0.9933	0.1412	0.7277	0.2593

(**Alignment**): CLIPScore [31], ImageReward [49], PicScore [14], and HPSv2 [47]. Effective models should have lower BRISQUE and higher scores for other quality indicators.

For quality assessment, we apply 12 advanced quality indicators for comparison, as (**Perceptual**) DBCNN [52], CLIPQA [39], CNNIQA [11], HyperIQA [37], NIMA [38], and Paq-2-Piq [51]; (**Alignment**) CLIPScore [31], ImageReward [49], HPSv1 [48], HPSv2 [47], and CLIP-Surgery [23]. We measure the correlation between subjective labeling objective prediction, namely Spearman Rank-order Correlation Coefficient (SRCC) and Pearson Linear Correlation Coefficient (PLCC). Higher SRCC/PLCC indicates better prediction monotonicity/accuracy. All quality indicators are fine-tuned on the AIGQA-20K (training set). During the training process of PQ-Map, we froze the parameters of the image encoder as CLIP-Surgery [23] and only updated the text encoder. While for the AQ-Map, the parameters of the image encoder are initialized as ImageReward [49]. The refiner Stage 1 adapts SDXL-Inpainting [35] model mixing PQ/AQ-Map as a mask; Stage 2 applies PASD [50] model globally. Each stage takes half of the iterations. We generate original AIGs and train quality indicators for 50 epochs using Adam optimizer on a server with four NVIDIA RTX A6000, and validate the quality optimization/assessment performance on a local NVIDIA GeForce RTX 4090.

4.3 Quality Optimization Results

Table 2, 3, 4, and 5 listed the perceptual/alignment quality optimization result. G-Refine’s advantages are primarily showcased in its **superior positive optimization** capabilities for AIGI quality. Across 13 indicators assessed on 4 databases, G-Refine secured first or second place in over 90% of the cases (47/52). The performance is more exceptional on the standard AIGI database GenImage, and the AIGQA-3K with significant internal quality variation. Though StableSR and SDXL also exhibit certain optimization for perceptual and alignment quality, G-Refine stands out by offering general optimization for both qualities. G-Refine’s ability to excel in BRISQUE and LIQE, which represent signal fidelity and aesthetics, respectively, underscores its multi-dimensional perceptual quality optimization. Similarly, its dominance in CLIP and ImageReward, indicative of word-level and sentence-level semantic alignment, demonstrates its capacity to understand and enhance word relationships for images. Considering some indicators are inconsistent with human real preferences, to enhance the credibility of real scenarios, we considered the indicators most relevant to human subjective preferences [43–46], namely Q-Align and HPSv2. Notably, G-Refine achieved the best in both, indicating its ability to enhance human genuine contentment with AIGs beyond fixed indicators.

Table 4: Using different quality optimizer on AGIQA-1K database. Abbreviation and keys follow Table 2.

Optimizer	Method / Indicator	CLIPQA↑	UNIQUE↑	LIQE↑	DBCNN↑	TOPIQ↑	CNNQA↑	MUSIQ↑	BRISQ↓	Q-Align↑	CLIPS↑	ImgRw↑	PicS↑	HPSv2↑
N/A	<i>Original Images</i>	0.6314	1.2237	3.6079	0.5730	0.5386	0.6332	68.330	31.727	3.5527	0.6648	-1.4530	0.4079	0.2465
Restoration	RFDN (ECCV2020)	0.6324	1.2249	3.6054	0.5732	0.6338	0.6383	68.304	31.754	3.5566	0.6617	-1.4509	0.4077	0.2464
	Swin2SR (ECCV2022)	0.6374	1.2250	3.6076	0.5746	0.6397	0.6285	68.365	31.515	3.5566	0.6659	-1.4522	0.4083	0.2465
	StableSR (Arxiv2023)	0.7664	1.5365	4.4375	0.7128	0.7233	0.7597	75.111	14.401	3.9629	0.7025	-1.4702	0.4435	0.2489
	DASR (CVPR2021)	0.6337	1.0618	3.3594	0.6271	0.5470	0.6933	62.765	45.635	3.3086	0.6663	-1.4715	0.3990	0.2464
Reconstruct -ion	SD-Upscale (CVPR2022)	0.6262	1.2746	3.7111	0.5578	0.5477	0.6236	69.246	36.646	3.5488	0.6694	-1.4621	0.4086	0.2463
	Instructpix (CVPR2023)	0.6306	1.1273	3.4683	0.5646	0.5261	0.6330	75.321	31.365	3.4824	0.6564	-1.4671	0.4031	0.2465
	DiffBIR (Arxiv2024)	0.6994	1.8592	4.3359	0.6539	0.6482	0.6855	77.562	27.518	3.9258	0.6905	-1.5073	0.4389	0.2455
	PASD (Arxiv2024)	0.6926	1.5653	4.3969	0.6829	0.6875	0.6532	73.684	23.431	3.9453	0.6899	-1.5007	0.4230	0.2445
Refinement	SDXL-Refiner (ICLR2023)	0.7021	1.5065	4.3324	0.6185	0.5887	0.6550	76.521	52.893	3.9473	0.7841	-1.1106	0.5319	0.2523
	SD (CVPR2022)	0.6523	1.3299	3.7332	0.5827	0.5520	0.5702	69.585	26.675	3.5508	0.9366	-0.5347	0.5967	0.2561
	SDXL (ICLR2024)	0.5849	1.1592	3.6301	0.5251	0.5106	0.6161	68.755	36.184	3.6621	0.8261	-0.8687	0.5738	0.2527
	InstructIR (Arxiv2024)	0.6766	1.4906	4.2460	0.6287	0.6135	0.6810	72.514	33.462	3.8398	0.9703	-0.1914	0.6463	0.2584
	Q-Refine (ICME2024)	0.7394	1.6307	4.4129	0.6613	0.6486	0.6897	73.164	19.420	3.9785	0.9122	-1.3007	0.4563	0.2475
G-Refine (Ours)		0.7741	1.6773	4.6922	0.7351	0.7542	0.6594	76.487	9.3422	4.1703	0.9610	-0.3064	0.6704	0.2611

Table 5: Using different quality optimizer on AGIQA-3K database. Abbreviation and keys follow Table 2.

Optimizer	Method / Indicator	CLIPQA↑	UNIQUE↑	LIQE↑	DBCNN↑	TOPIQ↑	CNNQA↑	MUSIQ↑	BRISQ↓	Q-Align↑	CLIPS↑	ImgRw↑	PicS↑	HPSv2↑
N/A	<i>Original Images</i>	0.5941	0.9001	3.3994	0.5330	0.5187	0.5856	60.740	35.261	3.7500	0.9527	-0.0727	0.6849	0.2508
Restoration	RFDN (ECCV2020)	0.5929	0.8986	3.3971	0.5325	0.5817	0.5867	60.713	35.197	3.7520	0.9521	-0.0716	0.6849	0.2507
	Swin2SR (ECCV2022)	0.5996	0.9010	3.3997	0.5344	0.5195	0.5857	60.725	35.167	3.7559	0.9529	-0.0710	0.6852	0.2465
	StableSR (Arxiv2023)	0.7453	1.3792	4.1906	0.6849	0.6805	0.7090	70.516	11.496	4.2539	0.9555	-0.1249	0.7030	0.2539
	DASR (CVPR2021)	0.5302	0.5361	2.8626	0.5611	0.5079	0.6993	57.476	53.068	3.0566	0.9510	-0.1927	0.6470	0.2490
Reconstruct -ion	SD-Upscale (CVPR2022)	0.5884	0.9373	3.4210	0.5196	0.5188	0.5977	62.294	35.139	3.8809	0.9449	-0.1204	0.6771	0.2501
	Instructpix (CVPR2023)	0.5876	0.8473	3.3395	0.5212	0.5047	0.5958	69.330	35.132	3.6680	0.9448	-0.1179	0.6705	0.2510
	DiffBIR (Arxiv2024)	0.6734	1.1664	3.7956	0.6358	0.6536	0.6815	67.950	15.634	4.1094	0.9608	-0.1979	0.6796	0.2514
	PASD (Arxiv2024)	0.7161	1.8243	3.9960	0.6258	0.6372	0.6535	65.630	24.230	4.1222	0.9673	-0.1674	0.7067	0.2521
Refinement	SDXL-Refiner (ICLR2023)	0.6694	1.2785	3.9161	0.5497	0.5372	0.6527	66.365	28.948	3.4399	0.9598	0.1350	0.7597	0.2523
	SD (CVPR2022)	0.6267	1.0776	3.6229	0.5299	0.5147	0.5702	64.414	30.296	3.7109	0.9595	0.1083	0.7187	0.2538
	SDXL (ICLR2023)	0.5358	0.7406	3.1452	0.4486	0.4610	0.5310	59.397	41.067	3.8652	0.9749	0.2310	0.7697	0.2527
	InstructIR (Arxiv2024)	0.6526	1.0183	3.6662	0.5666	0.5587	0.6207	63.344	39.948	3.8691	0.9934	0.0311	0.7009	0.2532
	Q-Refine (ICME2024)	0.7183	1.1291	3.7658	0.5990	0.5735	0.6539	89.897	22.001	4.1367	0.9783	-0.0992	0.7027	0.2521
G-Refine (Ours)		0.7717	1.5990	4.5163	0.7099	0.7168	0.6891	73.551	8.0697	4.3198	0.9865	0.2663	0.7643	0.2589

Another key strength of G-Refine lies in its *minimized negative optimization*. On 52 indexes, we marked results with lower quality than the original image. It can be seen that almost all other methods have experienced more than 10 negative optimizations (only Q-Refine has less negative optimization but at the cost of limited positive optimization). In contrast, G-Refine produced only one negative optimization. This superiority stems from G-Refine’s superior control over optimization intensity. Traditional methods often struggle to strike a balance, as enhancing LQ inevitably leads to degradation in HQ regions. However, G-Refine demonstrates a unique capability, achieving just one negative optimization. This demonstrates its capacity to discern between LQ and HQ regions, performing targeted, moderate denoising of defective areas without resorting to global operations.

Considering the above four databases are all generated by traditional, single T2I models, Figure 6 shows the performance⁵ of the above optimizers on a variety of advanced T2I models, containing AnimateDiff [9], DALLE2 [32], Dreamlike [8], IF [7], PixArt [3], SD1.5 [34], SD Cascade [28], and SDXL [35]. Intriguingly, G-Refine exhibits a stronger impact on models with lower initial quality, with notable collaborative optimization of perceptual/alignment quality for AnimateDiff, Dreamlike, SD1.5, and SD Cascade. For models

with higher original generation quality, G-Refine still leads in perceptual quality, but the alignment optimization is less pronounced, particularly for PixArt, where all optimizers, including G-Refine, negatively affect alignment. Consequently, given the success of G-Refine with traditional models, exploring further optimization of advanced models’ generative quality (especially for alignment) is a pertinent research question.

4.4 Quality Assessment Results

The two sub-modules of G-Refine, namely PQ/AQ-Map, can also be used independently for quality evaluation tasks. Tables 6 and 7 illustrate their performance on AIGI-20K and cross-validated with AGIQA-3K. The existing methods generally excel in providing accurate quality scores, but are unable to offer quality maps. On the other hand, methods that support quality maps as outputs often have unacceptable correlations with human subjective ratings, rendering them less practical. PQ-Map and AQ-Map stand out in this regard, as they not only offer accurate scores but also produce quality maps that are both usable and comparable to the most advanced models in terms of perception and alignment quality evaluation. Their ability to output quality maps makes them highly applicable in tasks such as image annotation and restoration, with G-Refine serving as a prime example. We are eager to see the potential for these maps to be further integrated into related fields.

⁵To simplify the image structure, we selected the three best-performing optimizers in Table 2-5 along with the original image for comparison.

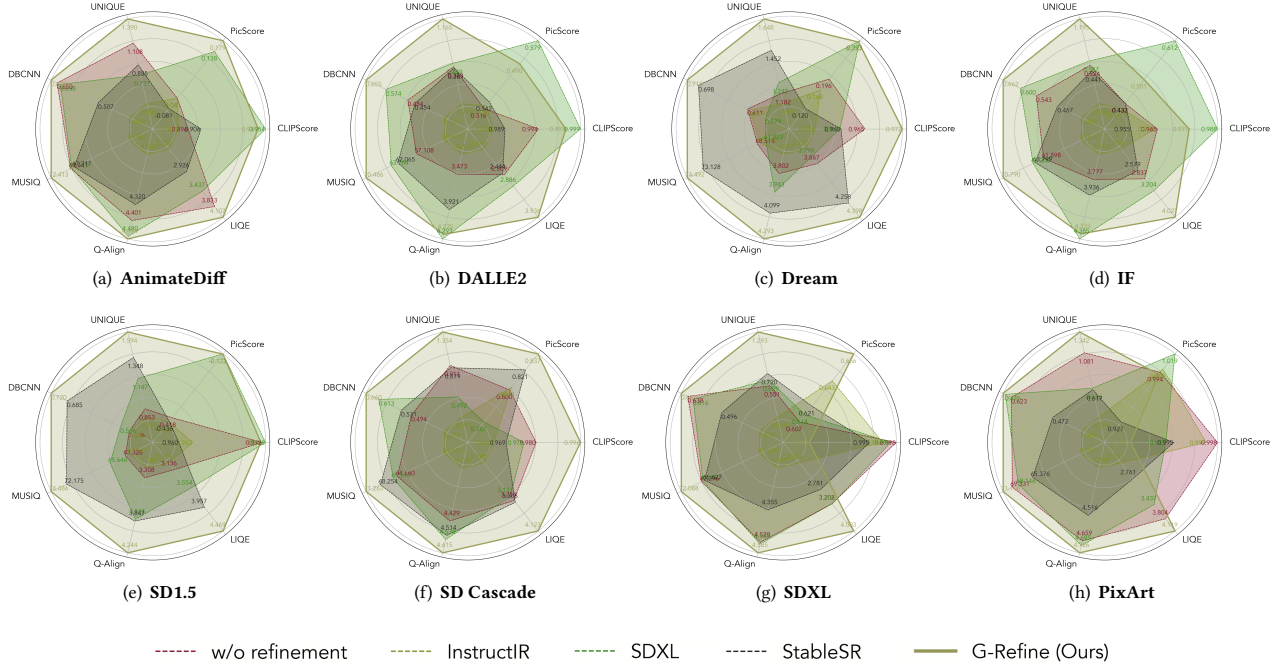


Figure 6: Radar maps for G-Refine on different original generative models.

Table 6: Perceptual quality assessment result of PQ-Map and different indicators. [Key: Best; Below 0.6]

Database Method	AIGI-20K		AGIQA-3K		#Support Map?
	SROCC	PLCC	SROCC	PLCC	
DBCNN	0.8506	0.8688	0.7488	0.7407	✗
CLIPQA	0.7500	0.6375	0.6364	0.4518	✗
CNN-IQA	0.5968	0.5483	0.5913	0.5418	✗
HyperIQA	0.8223	0.5209	0.8407	0.4901	✗
NIMA	0.8466	0.7851	0.8764	0.7954	✗
Paq2Piq	0.1709	0.5030	0.2928	0.5727	✓
PQ-Map (Proposed)	0.7073	0.6910	0.7054	0.7084	✓

Table 7: Alignment quality assessment result of AQ-Map and different indicators. [Key: Best; Below 0.6]

Database Method	AIGI-20K		AGIQA-3K		#Support Map?
	SROCC	PLCC	SROCC	PLCC	
CLIPScore	0.4033	0.4903	0.4701	0.5341	✗
ImageReward	0.6113	0.6620	0.7298	0.7862	✗
HPS	0.5550	0.4971	0.6349	0.7000	✗
HPSv2	0.6053	0.6385	0.6061	0.7164	✗
PicScore	0.5923	0.6106	0.6977	0.7633	✗
CLIP Surgery	0.4160	0.5225	0.5441	0.6648	✓
AQ-Map (Proposed)	0.6117	0.6797	0.7303	0.7862	✓

4.5 Ablation Study

To assess the individual impact of the two stages in G-Refine and the guidance provided by PQ/AQ-Map, we temporarily disabled stage 2 and excluded these components in Table 8. The result demonstrates the optimization effect, with Q-Align [45] and PicScore [14] representing perceptual/alignment quality respectively.

Table 8: Using G-Refine to optimize traditional and emerging generative models with different original quality. Abandoning PQ/AQ-Map as indicators, and deactivating Stage 2.

Database Indicator Stage		SD1.5		SD Cascade	
		PicScore	Q-Align	PicScore	Q-Align
PQ+AQ	1,2	-0.1216	4.2436	0.8371	4.6149
AQ	1,2	-0.1914	3.9463	0.8647	4.4621
PQ	1,2	-0.2481	4.0368	0.8072	4.5983
PQ+AQ	1	-0.2399	4.0409	0.8133	4.4690
Original Images		-0.4183	3.3082	0.8003	4.4294

On SD1.5 with lower original quality, stage 1 plays a significant role in the optimization process. Conversely, on SD Cascade, which has a higher quality initially, the contribution of stage 1 is less pronounced and stage 2 becomes the primary driver of improvement.

When using only one quality map, they excel in enhancing perceptual or alignment quality individually, but their combined effect on the other aspect is less effective. This highlights the importance of integrating both stages and utilizing both indicators for a comprehensive optimization of traditional and advanced T2I models, ensuring general optimization in perceptual/alignment quality.

5 CONCLUSION

In this study, we address the inconsistent generative quality of T2I models by proposing a quality-inspired general optimizer. Firstly, we enhance the CLIP’s image and text encoders towards accurate perceptual quality maps for AIGIs. Secondly, we analyze prompts using a syntax tree, employing an ancestor tracing mechanism to

yield alignment quality maps. Lastly, for precise and moderate optimization, these maps are employed to guide a multi-stage denoising process for AIGIS. These meticulously designed pipelines work in synergy to boost positive optimization for LQ while minimizing the negative impact on HQ images. Experimental results demonstrate that G-Refine improves AIGI's quality across 13 perceptual and alignment indicators and effectiveness to various T2I models, facilitating the adoption of T2I models in industrial production.

REFERENCES

- [1] Tim Brooks, Aleksander Holynski, and Alexei A Efros. 2023. Instructpix2pix: Learning to follow image editing instructions. In *Proceedings of the IEEE/CVF Conference on Computer Vision and Pattern Recognition*. 18392–18402.
- [2] Chaofeng Chen, Jiadi Mo, Jingwen Hou, Haoning Wu, Liang Liao, Wenxiu Sun, Qiong Yan, and Weisi Lin. 2023. TOPIQ: A Top-down Approach from Semantics to Distortions for Image Quality Assessment. arXiv:2308.03060 [cs.CV]
- [3] Junsong Chen, Jincheng Yu, Chongjian Ge, Lewei Yao, Enze Xie, Yue Wu, Zhongdao Wang, James Kwok, Ping Luo, Huchuan Lu, and Zhenguo Li. 2023. PixArt- α : Fast Training of Diffusion Transformer for Photorealistic Text-to-Image Synthesis. 2310.00426.
- [4] Zijian Chen, Wei Sun, Haoning Wu, Zicheng Zhang, Jun Jia, Zhongpeng Ji, Fengyu Sun, Shangling Jui, Xiongkuo Min, Guangtao Zhai, and Wenjun Zhang. 2024. Exploring the Naturalness of AI-Generated Images. arXiv:2312.05476 [cs.CV]
- [5] Marcos V Conde, Ui-Jin Choi, Maxime Burchi, and Radu Timofte. 2022. Swin2sr: Swin2 transformer for compressed image super-resolution and restoration. In *European Conference on Computer Vision*. Springer, 669–687.
- [6] Marcos V. Conde, Gregor Geigle, and Radu Timofte. 2024. InstructIR: High-Quality Image Restoration Following Human Instructions. arXiv:2401.16468 [cs.CV]
- [7] DeepFloyd. 2023. IF-I-XL-v1.0. <https://www.deepfloyd.ai>.
- [8] dreamlike art. 2023. dreamlike-photoreal-2.0. <https://dreamlike.art>.
- [9] Yuwei Guo, Ceyuan Yang, Anyi Rao, Zhengyang Liang, Yaohui Wang, Yu Qiao, Maneesh Agrawala, Dahua Lin, and Bo Dai. 2024. AnimateDiff: Animate Your Personalized Text-to-Image Diffusion Models without Specific Tuning. *International Conference on Learning Representations* (2024).
- [10] Xinhui Huang, Chunyi Li, Abdelhak Bentaleb, Roger Zimmermann, and Guangtao Zhai. 2023. XGC-VQA: A Unified Video Quality Assessment Model for User, Professionally, and Occupationally-Generated Content. In *IEEE International Conference on Multimedia and Expo Workshops*.
- [11] Le Kang, Peng Ye, Yi Li, and David Doermann. 2014. Convolutional neural networks for no-reference image quality assessment. In *Proceedings of the IEEE conference on computer vision and pattern recognition*. 1733–1740.
- [12] Junjie Ke, Qifei Wang, Yilin Wang, Peyman Milanfar, and Feng Yang. 2021. Musiq: Multi-scale image quality transformer. In *Proceedings of the IEEE/CVF international conference on computer vision*. 5148–5157.
- [13] Alexander Kirillov, Eric Mintun, Nikhila Ravi, Hanzi Mao, Chloe Rolland, Laura Gustafson, Tete Xiao, Spencer Whitehead, Alexander C Berg, Wan-Yen Lo, et al. 2023. Segment anything. In *Proceedings of the IEEE/CVF International Conference on Computer Vision*. 4015–4026.
- [14] Yuval Kirstain, Adam Polyak, Uriel Singer, Shahbuland Matiana, Joe Penna, and Omer Levy. 2024. Pick-a-pic: An open dataset of user preferences for text-to-image generation. *Advances in Neural Information Processing Systems* 36 (2024).
- [15] Tengchuan Kou, Xiaohong Liu, Zicheng Zhang, Chunyi Li, Haoning Wu, Xiongkuo Min, Guangtao Zhai, and Ning Liu. 2024. Subjective-Aligned Dataset and Metric for Text-to-Video Quality Assessment. arXiv:2403.11956 [cs.CV]
- [16] Chunyi Li, Tengchuan Kou, Yixuan Gao, Yuqin Cao, Wei Sun, Zicheng Zhang, Yingjie Zhou, Zhichao Zhang, Weixia Zhang, Haoning Wu, Xiaohong Liu, Xiongkuo Min, and Guangtao Zhai. 2024. AIGQA-20K: A Large Database for AI-Generated Image Quality Assessment. arXiv:2404.03407 [cs.CV]
- [17] Chunyi Li, May Lim, Abdelhak Bentaleb, and Roger Zimmermann. 2023. A Real-Time Blind Quality-of-Experience Assessment Metric for HTTP Adaptive Streaming. In *IEEE International Conference on Multimedia and Expo*.
- [18] Chunyi Li, Guo Lu, Donghui Feng, Haoning Wu, Zicheng Zhang, Xiaohong Liu, Guangtao Zhai, Weisi Lin, and Wenjun Zhang. 2024. MISC: Ultra-low Bitrate Image Semantic Compression Driven by Large Multimodal Model. arXiv:2402.16749 [cs.CV]
- [19] Chunyi Li, Haoning Wu, Zicheng Zhang, Hongkun Hao, Kaiwei Zhang, Lei Bai, Xiaohong Liu, Xiongkuo Min, Weisi Lin, and Guangtao Zhai. 2024. Q-Refine: A Perceptual Quality Refiner for AI-Generated Image. arXiv:2401.01117 [cs.CV]
- [20] Chunyi Li, Zicheng Zhang, Wei Sun, Xiongkuo Min, and Guangtao Zhai. 2022. A Full-Reference Quality Assessment Metric for Cartoon Images. In *IEEE 24th International Workshop on Multimedia Signal Processing*.
- [21] Chunyi Li, Zicheng Zhang, Haoning Wu, Wei Sun, Xiongkuo Min, Xiaohong Liu, Guangtao Zhai, and Weisi Lin. 2023. AGIQA-3K: An Open Database for AI-Generated Image Quality Assessment. *IEEE Transactions on Circuits and Systems for Video Technology* (2023).
- [22] Yanyu Li, Xian Liu, Anil Kag, Ju Hu, Yerlan Idelbayev, Dhritiman Sagar, Yanzhi Wang, Sergey Tulyakov, and Jian Ren. 2024. TextCrafter: Your Text Encoder Can be Image Quality Controller. arXiv:2403.18978 [cs.CV]
- [23] Yi Li, Hualiang Wang, Yiqun Duan, and Xiaomeng Li. 2023. CLIP Surgery for Better Explainability with Enhancement in Open-Vocabulary Tasks. arXiv:2304.05653 [cs.CV]
- [24] Xinqi Lin, Jingwen He, Ziyan Chen, Zhaoyang Lyu, Bo Dai, Fanghua Yu, Wanli Ouyang, Yu Qiao, and Chao Dong. 2024. DiffBIR: Towards Blind Image Restoration with Generative Diffusion Prior. arXiv:2308.15070 [cs.CV]
- [25] Jie Liu, Jie Tang, and Gangshan Wu. 2020. Residual feature distillation network for lightweight image super-resolution. In *Computer Vision—ECCV 2020 Workshops: Glasgow, UK, August 23–28, 2020, Proceedings, Part III* 16. Springer, 41–55.
- [26] Xiaohong Liu, Xiongkuo Min, Guangtao Zhai, Chunyi Li, Tengchuan Kou, Wei Sun, Haoning Wu, Yixuan Gao, Yuqin Cao, Zicheng Zhang, Xiele Wu, Radu Timofte, et al. 2024. NTIRE 2024 Quality Assessment of AI-Generated Content Challenge. In *Proceedings of the IEEE/CVF Conference on Computer Vision and Pattern Recognition (CVPR) Workshops*.
- [27] Anish Mittal, Anush Krishna Moorthy, and Alan Conrad Bovik. 2012. No-reference image quality assessment in the spatial domain. *IEEE Transactions on image processing* 21, 12 (2012), 4695–4708.
- [28] Pablo Pernias, Dominic Rampas, Mats Leon Richter, Christopher Pal, and Marc Aubreville. 2024. Würstchen: An Efficient Architecture for Large-Scale Text-to-Image Diffusion Models. In *The Twelfth International Conference on Learning Representations*.
- [29] Dustin Podell, Zion English, Kyle Lacey, Andreas Blattmann, Tim Dockhorn, Jonas Müller, Joe Penna, and Robin Rombach. 2023. SDXL: Improving Latent Diffusion Models for High-Resolution Image Synthesis. arXiv:2307.01952 [cs.CV]
- [30] Leigang Qu, Wenjie Wang, Yongqi Li, Hanwang Zhang, Liqiang Nie, and Tat-Seng Chua. 2024. Discriminative Probing and Tuning for Text-to-Image Generation. arXiv:2403.04321 [cs.CV]
- [31] Alec Radford, Jong Wook Kim, Chris Hallacy, Aditya Ramesh, Gabriel Goh, Sandhini Agarwal, Girish Sastry, Amanda Askell, Pamela Mishkin, Jack Clark, et al. 2021. Learning transferable visual models from natural language supervision. In *International conference on machine learning*. PMLR, 8748–8763.
- [32] Aditya Ramesh, Prafulla Dhariwal, Alex Nichol, Casey Chu, and Mark Chen. 2022. Hierarchical Text-Conditional Image Generation with CLIP Latents. 2204.06125.
- [33] Yongming Rao, Wenliang Zhao, Guangyi Chen, Yansong Tang, Zheng Zhu, Guan Huang, Jie Zhou, and Jiwen Lu. 2022. Densclip: Language-guided dense prediction with context-aware prompting. In *Proceedings of the IEEE/CVF conference on computer vision and pattern recognition*. 18082–18091.
- [34] Robin Rombach, Andreas Blattmann, Dominik Lorenz, Patrick Esser, and Björn Ommer. 2022. High-resolution image synthesis with latent diffusion models. In *Proceedings of the IEEE/CVF conference on computer vision and pattern recognition*. 10684–10695.
- [35] Robin Rombach, Andreas Blattmann, and Björn Ommer. 2022. Text-Guided Synthesis of Artistic Images with Retrieval-Augmented Diffusion Models. 2207.13038.
- [36] Chenyang Si, Ziqi Huang, Yuming Jiang, and Ziwei Liu. 2023. FreeU: Free Lunch in Diffusion U-Net. arXiv:2309.11497 [cs.CV]
- [37] Shaolin Su, Qingsen Yan, Yu Zhu, Cheng Zhang, Xin Ge, Jinjia Sun, and Yanning Zhang. 2020. Blindly assess image quality in the wild guided by a self-adaptive hyper network. In *Proceedings of the IEEE/CVF Conference on Computer Vision and Pattern Recognition*. 3667–3676.
- [38] Hossein Talebi and Peyman Milanfar. 2018. NIMA: Neural image assessment. *IEEE transactions on image processing* 27, 8 (2018), 3998–4011.
- [39] Jianyi Wang, Kelvin CK Chan, and Chen Change Loy. 2023. Exploring clip for assessing the look and feel of images. In *Proceedings of the AAAI Conference on Artificial Intelligence*, Vol. 37. 2555–2563.
- [40] Jianyi Wang, Zongsheng Yue, Shangchen Zhou, Kelvin C. K. Chan, and Chen Change Loy. 2023. Exploiting Diffusion Prior for Real-World Image Super-Resolution. arXiv:2305.07015 [cs.CV]
- [41] Zijie J. Wang, Evan Montoya, David Munechika, Haoyang Yang, Benjamin Hoover, and Duen Horng Chau. 2023. DiffusionDB: A Large-scale Prompt Gallery Dataset for Text-to-Image Generative Models. In *Proceedings of the 61st Annual Meeting of the Association for Computational Linguistics (Volume 1: Long Papers)*. Association for Computational Linguistics, 893–911.
- [42] Yunxuan Wei, Shuhang Gu, Yawei Li, Radu Timofte, Longcun Jin, and Hengjie Song. 2021. Unsupervised real-world image super resolution via domain-distance aware training. In *Proceedings of the IEEE/CVF conference on computer vision and pattern recognition*. 13385–13394.
- [43] Haoning Wu, Zicheng Zhang, Erli Zhang, Chaofeng Chen, Liang Liao, Annan Wang, Chunyi Li, Wenxiu Sun, Qiong Yan, Guangtao Zhai, et al. 2023. Q-Bench: A Benchmark for General-Purpose Foundation Models on Low-level Vision. arXiv:2309.14181 [cs.CV]
- [44] Haoning Wu, Zicheng Zhang, Erli Zhang, Chaofeng Chen, Liang Liao, Annan Wang, Kaixin Xu, Chunyi Li, Jingwen Hou, Guangtao Zhai, et al. 2023. Q-instruct: Improving low-level visual abilities for multi-modality foundation models. arXiv:2311.06783 [cs.CV]

- [45] Haoning Wu, Zicheng Zhang, Weixia Zhang, Chaofeng Chen, Liang Liao, Chunyi Li, Yixuan Gao, Annan Wang, Erli Zhang, Wenxiu Sun, et al. 2023. Q-Align: Teaching LMMs for Visual Scoring via Discrete Text-Defined Levels. arXiv:2312.17090 [cs.CV]
- [46] Haoning Wu, Hanwei Zhu, Zicheng Zhang, Erli Zhang, Chaofeng Chen, Liang Liao, Chunyi Li, Annan Wang, Wenxiu Sun, Qiong Yan, Xiaohong Liu, Guangtao Zhai, Shiqi Wang, and Weisi Lin. 2024. Towards Open-ended Visual Quality Comparison. arXiv:2402.16641 [cs.CV]
- [47] Xiaoshi Wu, Yiming Hao, Keqiang Sun, Yixiong Chen, Feng Zhu, Rui Zhao, and Hongsheng Li. 2023. Human Preference Score v2: A Solid Benchmark for Evaluating Human Preferences of Text-to-Image Synthesis. arXiv:2306.09341 [cs.CV]
- [48] Xiaoshi Wu, Keqiang Sun, Feng Zhu, Rui Zhao, and Hongsheng Li. 2023. Human preference score: Better aligning text-to-image models with human preference. In *Proceedings of the IEEE/CVF International Conference on Computer Vision*. 2096–2105.
- [49] Jiazhen Xu, Xiao Liu, Yuchen Wu, Yuxuan Tong, Qinkai Li, Ming Ding, Jie Tang, and Yuxiao Dong. 2024. Imagereward: Learning and evaluating human preferences for text-to-image generation. *Advances in Neural Information Processing Systems* 36 (2024).
- [50] Tao Yang, Rongyuan Wu, Peiran Ren, Xuansong Xie, and Lei Zhang. 2024. Pixel-Aware Stable Diffusion for Realistic Image Super-resolution and Personalized Stylization. arXiv:2308.14469 [cs.CV]
- [51] Zhenqiang Ying, Haoran Niu, Praful Gupta, Dhruv Mahajan, Deepti Ghadiyaram, and Alan Bovik. 2020. From Patches to Pictures (PaQ-2-PiQ): Mapping the Perceptual Space of Picture Quality. In *Proceedings of the IEEE/CVF Computer Vision and Pattern Recognition*.
- [52] Weixia Zhang, Kede Ma, Jia Yan, Dexiang Deng, and Zhou Wang. 2018. Blind image quality assessment using a deep bilinear convolutional neural network. *IEEE Transactions on Circuits and Systems for Video Technology* 30, 1 (2018), 36–47.
- [53] Weixia Zhang, Kede Ma, Guangtao Zhai, and Xiaokang Yang. 2021. Uncertainty-aware blind image quality assessment in the laboratory and wild. *IEEE Transactions on Image Processing* 30 (2021), 3474–3486.
- [54] Weixia Zhang, Guangtao Zhai, Ying Wei, Xiaokang Yang, and Kede Ma. 2023. Blind image quality assessment via vision-language correspondence: A multitask learning perspective. In *Proceedings of the IEEE/CVF Conference on Computer Vision and Pattern Recognition*. 14071–14081.
- [55] Zicheng Zhang, Chunyi Li, Wei Sun, Xiaohong Liu, Xiongkuo Min, and Guangtao Zhai. 2023. A Perceptual Quality Assessment Exploration for AIGC Images. In *IEEE International Conference on Multimedia and Expo Workshops (ICMEW)*. 440–445.
- [56] Zicheng Zhang, Wei Sun, Haoning Wu, Yingjie Zhou, Chunyi Li, Zijian Chen, Xiongkuo Min, Guangtao Zhai, and Weisi Lin. 2023. Gms-3dqa: Projection-based grid mini-patch sampling for 3d model quality assessment. *ACM Transactions on Multimedia Computing, Communications and Applications* (2023).
- [57] Zicheng Zhang, Wei Sun, Yingjie Zhou, Haoning Wu, Chunyi Li, Xiongkuo Min, Xiaohong Liu, Guangtao Zhai, and Weisi Lin. 2023. Advancing Zero-Shot Digital Human Quality Assessment through Text-Prompted Evaluation. arXiv:2307.02808 [eess.IV]
- [58] Zicheng Zhang, Haoning Wu, Zhongpeng Ji, Chunyi Li, Erli Zhang, Wei Sun, Xiaohong Liu, Xiongkuo Min, Fengyu Sun, Shangling Jui, et al. 2023. Q-Boost: On Visual Quality Assessment Ability of Low-level Multi-Modality Foundation Models. arXiv:2312.15300 [cs.CV]
- [59] Zicheng Zhang, Yingjie Zhou, Long Teng, Wei Sun, Chunyi Li, Xiongkuo Min, Xiao-Ping Zhang, and Guangtao Zhai. 2024. Quality-of-Experience Evaluation for Digital Twins in 6G Network Environments. *IEEE Transactions on Broadcasting* (2024).
- [60] Mingjian Zhu, Hanting Chen, Qiangyu YAN, Xudong Huang, Guanyu Lin, Wei Li, Zhijun Tu, Hailin Hu, Jie Hu, and Yunhe Wang. 2023. GenImage: A Million-Scale Benchmark for Detecting AI-Generated Image. In *Advances in Neural Information Processing Systems*, A. Oh, T. Neumann, A. Globerson, K. Saenko, M. Hardt, and S. Levine (Eds.), Vol. 36. Curran Associates, Inc., 77771–77782.